

Using Molecular Embeddings in QSAR Modeling: Does it Make a Difference?

María Virginia Sabando,^{*,†,‡} Ignacio Ponzoni,^{†,‡} Evangelos E. Milios,[¶] and Axel J. Soto^{†,‡}

[†]*Institute for Computer Science and Engineering (UNS-CONICET), Bahía Blanca,
Argentina*

[‡]*Department of Computer Science and Engineering, Universidad Nacional del Sur, Bahía
Blanca, Argentina*

[¶]*Faculty of Computer Science, Dalhousie University, Halifax, NS, Canada*

E-mail: virginia.sabando@cs.uns.edu.ar

Abstract

Several novel algorithms for learning molecular representations have been proposed recently with the consolidation of deep learning in computer-aided drug design. Learned molecular embeddings allow attaining rich representations of the molecular structure and physical-chemical properties while overcoming several limitations of traditional molecular representations. Despite their theoretical benefits, it is not clear how molecular embeddings compare with each other and with traditional representations, which in turn hinders the process of choosing a suitable embedding algorithm for QSAR modeling. A reason for this lack of consensus is that a fair and thorough comparison of different approaches is not straightforward. To close this gap, we reproduced three unsupervised and two supervised molecular embedding techniques recently proposed in the literature. Through a thorough experimental setup, we compared the

molecular representations of these five methods concerning their performance in QSAR scenarios using five different datasets with varying class imbalance levels. We also compared these representations to traditional molecular representations, namely molecular descriptors and fingerprints. Our results show that molecular embeddings did not significantly surpass baseline results obtained using traditional molecular representations. While supervised techniques yielded competitive results compared to those obtained by traditional molecular representations, unsupervised techniques did not match the baseline results. Our results motivate a discussion about the usefulness of molecular embeddings in QSAR modeling and their potential in other drug design areas, such as similarity analysis and *de novo* drug design.

Introduction

Quantitative Structure-Activity Relationship (QSAR) models constitute the cornerstone of modern in silico drug discovery.¹ QSAR models are regression or classification models that predict the relationship between molecular features of compounds and a target property or bioactivity. They have been extensively used in modern computer-aided drug design to accelerate drug candidate identification while reducing costs associated with molecular synthesis and wet lab experiments. QSAR models are usually trained using traditional molecular representations, such as molecular descriptors and fingerprints built or computed using widely known algorithms on single compounds. Although these molecular representations are interpretable and often yield good classification results, they are limited in the molecular information they encode. For instance, molecular descriptors such as molecular weight or *cLogP* (partition coefficient octanol/water) value might have a high correlation to specific properties, such as water solubility or boiling point, but might not be appropriate for those tasks where capturing aspects of the molecular structure is crucial, such as molecular docking. Because of this, there is an increasing interest in exploring new, enriched representations that take into account multiple aspects of the molecule at once.²

Deep learning applied to Natural Language Processing (NLP) has experienced a prolific development during the last decade, and many techniques initially developed for text have been increasingly applied to other domains.^{3–5} In computer-aided drug design, research efforts have been put on designing novel techniques for learning rich molecular representations, yielding numerous novel algorithms for this task during the last years.^{2,3,6} In contrast to traditional molecular representations, learned molecular embeddings can be tailored to be low dimensional and versatile while still capturing diverse information about physical-chemical properties, molecular structure and bioactivity. Besides, unsupervised methods for obtaining molecular embeddings inspired by NLP techniques can be adapted to use widely available sequential representations of molecules, such as SMILES formulas.⁷ Therefore, such representations are promising as they can benefit from large ensembles of unlabeled compounds.

Algorithms for learning molecular embeddings employ a wide variety of state-of-the-art deep learning techniques,³ ranging from feed-forward neural-based autoencoders to graph neural networks^{5,8} and self-attention.⁹ Thus, molecular embedding algorithms vary in complexity and intricacy, allowing to tailor molecular embeddings to specific molecular informatics tasks. For example, many recent self-attention methods for molecular embeddings are designed to identify the molecular substructures that have a significant impact on the bioactivity profile.^{10,11} Nowadays, several QSAR modeling studies employ learned molecular embeddings instead of traditional molecular representations as training data. As depicted in Figure 1, molecular embeddings commonly consist of fixed-size dense vectors of real numbers, whereas traditional molecular representations can either consist of real number vectors or bit vectors varying in sparsity. These representations are fed to classification or regression models for QSAR modeling.

At learning time, molecular embeddings can either be *supervised*, meaning that they take into account labeled/external information about the bioactivity profile of the molecules towards a biological target under study, or *unsupervised*, which means that the embeddings are built with no human-labeled information. The main advantage of supervised embeddings

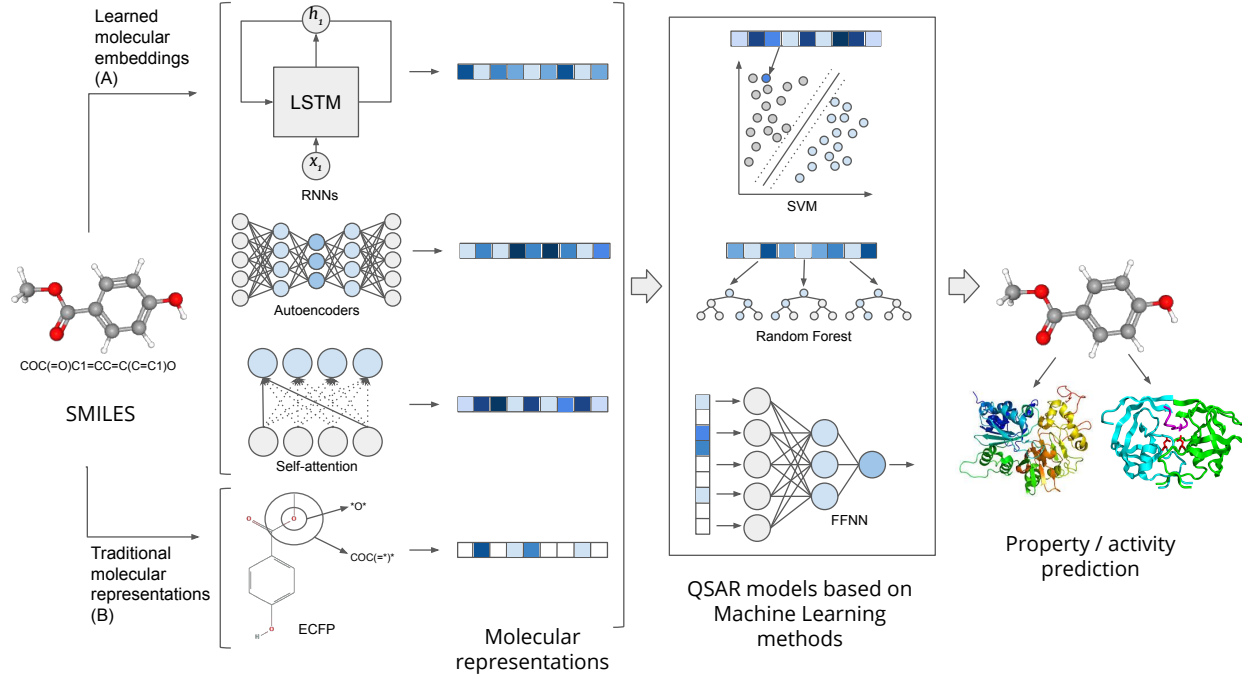


Figure 1: QSAR models can either be trained using learned molecular embeddings derived from deep learning and NLP techniques (A), or employing traditional molecular representations obtained from a *feature engineering* process (B). Molecular embeddings are dense vectors of real numbers vectors, whereas traditional molecular representations can be either real number vectors or bit vectors varying in sparsity. In turn, QSAR models are classification or regression models depending on the prediction task.

is that they encode bioactivity information, which could favor them in prediction tasks. However, they are consequently less flexible than unsupervised embeddings, since new embeddings need to be learned for different biological targets. Moreover, in order to learn supervised embeddings, it is necessary to have labeled datasets, which are often small and scarce, thus potentially impacting negatively on the quality of the embeddings.

Despite the proliferation of learned molecular representation methods, there is no benchmark or empirical research on choosing the most suitable representation method for QSAR analysis. Interestingly, some authors have presented results where learned molecular representations were not able to broadly surpass traditional representations in QSAR modeling.^{12–16} While establishing a fair comparison between molecular embeddings and traditional representations is not straightforward, we argue that such comparison is necessary and that it

needs to be carried out through an extensive experimental work that includes several state-of-the-art embedding methods. In order to establish a comparison on a fair ground, we propose a carefully designed evaluation where hyperparameters are optimized thoroughly, datasets of different characteristics are used, and several trials are run to account for their inherent stochasticity. In particular, this work aims to address the following research questions:

- Q1: Are molecular embeddings suitable as data representation for QSAR modeling? If so, do molecular embeddings outperform traditional molecular representations in a classification task?
- Q2: Does incorporating information about the biological target when computing the molecular embedding (supervised embeddings) incur higher classification performance than that obtained from unsupervised embeddings?
- Q3: Do different pre-processing decisions, such as the canonical form of the SMILES formulas used as training data or the size of the final embeddings, significantly impact on the classification performance of a QSAR model using molecular embeddings?

In this scenario, we conducted an extensive analysis of different molecular embedding techniques based on state-of-the-art deep learning methods concerning their suitability for QSAR modeling. We reproduced five recently proposed techniques: two of them belonging to the *supervised* category, whereas the remaining three are *unsupervised*. All five techniques and their models were trained using SMILES formulas as the raw molecular representation. To train the unsupervised methods, we employed a dataset of 40 million randomly selected and curated compounds retrieved from ZINC.¹⁷ In addition, we tested two different ways of computing canonical SMILES formulas in an effort to take advantage of the specific way of processing the SMILES formulae of each unsupervised technique. We trained different classifiers using five labeled datasets with varying class imbalance levels and size. Finally, we contrasted the performance attained by molecular embeddings to the baseline classification results obtained using traditional molecular representations. Our experimental workflow

consisted of over 20,000 runs, comprising several stages of model selection, replications and statistical analysis of the results.

Related Work

The trustworthiness of QSAR models and their predictive performance is linked to the choice of the molecular representation used for training.^{2,18,19} For this reason, many research efforts have been focused throughout the years on manually engineering high-quality molecular representations. This process, known as *feature engineering*, has led to widespread and commonly used molecular representations.^{20,21} Traditional molecular representations vary mostly in the type of information they encode and their usage depends on the specific task.^{22,23} Among the most commonly used traditional molecular representations, we can enumerate: *molecular descriptors*,²⁰ *Extended Connectivity Fingerprints (ECFPs)*²⁴ and *Molecular Access System (MACCS) keys*.²⁵

While a vast number of published QSAR models are based on these traditional representations,^{26–29} the process of obtaining such representations via feature engineering is costly, time-consuming, and requires strong domain-specific expertise. Moreover, since each of them encodes different information, there is no single representation suitable for every task. Traditional approaches for molecular representations often rely on a feature selection step, which introduces further design decisions before training a machine learning model.³⁰ Furthermore, modern cheminformatics methods show an increasing trend for the use of versatile molecular representations that capture the diversity of the chemical space.² Because of these reasons, many new methods for learning molecular representations have been developed recently, most of them based on deep learning techniques.^{2,3}

Recent methods for learning molecular embeddings employ *SMILES* formulas,⁷ which is the most widely used linear representation for encoding molecular graph information. Since SMILES formulas directly encode the molecular graph into a sequence of ASCII characters

using a depth-first graph traversal, they are suitable for deep learning techniques aimed at learning from sequential or graph-like data.³ Given their high availability—most molecular databases store the SMILES of each compound—, many unsupervised methods for learning molecular representations have been developed and trained on large databases without the need for labeled information.^{12,31–34} While images or structured graph representations have also been employed for learning molecular embeddings and QSAR modeling,^{14,35,36} their usage is not as widespread, and it has limitations in terms of data availability. Thus, in this paper, we focused on SMILES-based embedding methods.

The high availability of molecular data in SMILES format has motivated numerous approaches for learning molecular embeddings based on autoencoders, which enable to conduct unsupervised training procedures.^{12,13,34,37} In particular, Öztürk et al.³³ introduced *SMILESVec*, an unsupervised SMILES-based method that learns representations for small molecules using the popular *word2vec* model by Mikolov et al.³⁸ The authors performed a *tokenization* step onto a dataset of SMILES formulas—i.e., converted each SMILES into a string of distinguishable tokens in an alphabet— by computing overlapping SMILES substrings, which were then used to train their model. Finally, they computed the embedding of each molecule in the corpus by averaging the learned vectors for each of the tokens in its SMILES formula. Jaeger et al.¹² presented *Mol2Vec*, which is also based on *word2vec*.³⁸ In this latter method, SMILES formulas undergo a preprocessing stage before being fed to the auto-encoder, consisting of tokenizing the SMILES formulas using the algorithm commonly employed for computing ECFPs.²⁴ After an unsupervised training phase, the final representations are computed by summing the embedded vectors of all tokens in the molecule. The preprocessing step carried out by this method involves exploring the topology of the molecule in a circular way, which resembles the way Graph Neural Networks (GNNs) learn from the topology of graph-like data.³⁹

Since SMILES is a linear molecular notation of sequential nature, methods for either generating new molecules or learning new molecular embeddings based on Recurrent Neu-

ral Networks (RNNs) are also found in the literature.^{34,40,41} Most generative models in the literature are based on RNN auto-encoders trained on large sets of unlabeled data,³ which constitutes an interesting approach for learning molecular representations given that they capture the graph information encoded throughout the whole SMILES string. In this direction, Xu et al.³⁴ proposed *Seq2Seq Fingerprint*, an unsupervised method based on a recurrent auto-encoder built using bidirectional Long-Short Term Memory cells (LSTMs).⁴² *Seq2Seq Fingerprint* learns directly from SMILES formulas leveraging information from long-term dependencies and sequential relationships between their characters. The molecular embeddings are finally obtained by concatenating the hidden states of the BiLSTM RNN encoder.

Another trend in learned molecular representations is the use of self-attention,⁹ which enables to capture rich information about the molecule and identify relevant substructures to specific bioactivity traits while avoiding lengthy training procedures, in contrast to RNNs.⁹ In a sense, self-attention relates strongly to the way GNNs operate on graph-like data⁴³ but allowing to train on sequence data such as SMILES formulas. Thus, it constitutes an interesting approach for learning molecular representations. In this direction, Oskooei et al.¹¹ developed *PaccMann*, a novel approach for predicting anticancer compound sensitivity by means of multi-modal attention-based neural networks. The authors proposed a series of supervised encoders; the best performing one was a self-attentive encoder trained using a simple tokenization of SMILES strings and complemented with gene expression information. A shallow feed-forward neural network for property prediction was stacked to the embedding model so that the molecular embeddings were learned during the training phase of the classifier. Zheng et al.¹⁰ developed *SA-BiLSTM*, a supervised method based on a stack of a BiLSTM RNN and a self-attention mechanism, which yields self-attentive embeddings. This model is then plugged into a shallow feed-forward neural network for property prediction, and embeddings are learned along with the classification task. One interesting aspect of this method is that it does not learn from SMILES formulas directly but instead uses sequences of token embeddings from a pre-trained *Mol2Vec* model.¹² Wang et al.⁴⁴ developed *SMILES-*

BERT, a semi-supervised model consisting of a Transformer Layer⁹ trained using a large unlabeled dataset through a masked SMILES recovery task, as in the popular NLP *BERT* architecture.⁴⁵ This model can be then fine-tuned by means of a labeled dataset. Although *SMILES-BERT* seems a promising approach, important implementation details are missing to fully reproduce the method, especially in terms of the fine-tuning stage.

Materials and Methods

In this section, we describe the datasets and their preprocessing stage applied in this paper. Given the importance of the reproducibility of this paper, we provide a thorough explanation of our experimental setup and a workflow overview, including the neural architectures of the five methods we reproduced and their training. Finally, we provide details on the metrics chosen for evaluating and comparing the methods. All data and source code used in this paper are either cited to the original reference or made publicly available to facilitate the reproducibility of our work. In addition, all trained embedding models are also available so that they can be readily used. Further details can be found in “Data and Software Availability” section of this paper.

Datasets

Following the steps needed to reproduce the unsupervised techniques, we collected and downloaded the SMILES formulas of approximately 200 million purchasable compounds from ZINC.¹⁷ We conducted a preprocessing stage onto these compounds that consisted of filtering out compounds that did not comply with Lipinski’s Rule of 5.⁴⁶ We only kept compounds having a molecular weight between 12 and 600, heavy atom count between 3 and 50 and *cLogP* (partition coefficient octanol/water) value between -5 and 7. We also filtered out compounds that presented non-drug-like atoms, such as heavy metals, and removed salts and solvents. Finally, we obtained the canonical SMILES formulas for each of the remaining

compounds. This whole process was carried out using RDKit.⁴⁷ After the preprocessing stage, we randomly selected a subset of 40 million compounds, which were later used to train the unsupervised methods.

We also chose five different labeled datasets, which we describe below. These datasets were used to train the supervised methods and evaluate all of the embedding methods in a classification task. All of these datasets pose binary classification problems. We prioritized datasets that had initially been used to evaluate any of the reproduced methods by their authors while we accounted for diversity of sizes and class imbalance scenarios. The selected datasets were preprocessed following the same procedure used for ZINC. Further details about their class imbalance and numbers of compounds are summarized in Table 1. Namely, these datasets are:

- *SR-ARE*, a bioassay for small molecule agonists of the antioxidant response element (ARE) signaling pathwayⁱ. This assay of data is contained in the *Tox21 challenge* dataset, consisting of qualitative toxicity measurements on twelve biological targetsⁱⁱ.
- *SR-MMP*, a stress response assay for small molecule disruptors of the mitochondrial membrane potential (MMP)ⁱⁱⁱ. This dataset is also included in the *Tox21 challenge* dataset.
- *SR-ATAD5*, a set of small molecules that induce genotoxicity in human embryonic kidney cells expressing luciferase-tagged ATAD5^{iv}. This dataset also belongs to the *Tox21 challenge* dataset.
- *HIV*, a dataset introduced by the Drug Therapeutics Program (DTP) AIDS Antiviral Screen containing information about molecular ability to inhibit HIV replication. Screening results were categorized as confirmed inactive (CI), confirmed active (CA)

ⁱ<https://pubchem.ncbi.nlm.nih.gov/bioassay/743219>

ⁱⁱ<https://tripod.nih.gov/tox21/challenge/about.jsp>

ⁱⁱⁱ<https://pubchem.ncbi.nlm.nih.gov/bioassay/720637>

^{iv}<https://pubchem.ncbi.nlm.nih.gov/bioassay/720516>

and confirmed moderately active (CM). We merged the compounds categorized under the latter two labels, which yielded two classes: inactive (CI) and active (CA and CM)^v.

- *PCBA-686978*, a PubChem bioassay containing information about molecular ability to inhibit the human tyrosyl-DNA phosphodiesterase 1 (TDP1)^{vi}.

Table 1: Details of labeled datasets. The imbalance ratio is computed as the number of active compounds every 100 inactive compounds.

Dataset	# Compounds	# Active	# Inactive	Imbalance ratio
SR-ARE	5956	941	5015	18.76
SR-MMP	5937	925	5012	3.68
SR-ATAD5	7251	258	6993	18.46
HIV	41127	1443	39684	27.50
PCBA-686978	302175	62800	239375	3.81

Molecular Embedding Methods

Based on the scenario described in the previous section and after identifying the most prominent deep learning techniques for learning molecular representations based on SMILES formulas, we chose *SMILESVec*,³³ *Mol2Vec*,¹² *Seq2Seq Fingerprint*³⁴— which we refer to as *Seq2Seq* in this paper—, *PaccMann*’s self attentive encoder¹¹—named *PaccMann* throughout this paper— and *SA-BiLSTM* encoder by Zheng et al.¹⁰ as our reference embedding methods. We decided not to experiment with *SMILES-BERT*, due to the reproducibility issues pointed out in the previous section and because both *SA-BiLSTM* and *PaccMann* are also self-attention-based encoders. We selected these methods to test different deep learning architectures, model sizes in terms of trainable parameters and considering both supervised and unsupervised training scenarios. The goal of our experimental process was to thoroughly test each of the embedding methods and their suitability for QSAR modeling while at the

^v<https://wiki.nci.nih.gov/display/NCIDTPdata/AIDS+Antiviral+Screen+Data>

^{vi}<https://pubchem.ncbi.nlm.nih.gov/bioassay/686978>

same time taking into consideration different aspects that might influence their performance. Moreover, we aimed to perform a training phase consisting of multiple runs of each method in order to account for their intrinsic variance. For these reasons, we conducted our benchmarking process by testing an extensive range of combinations of hyperparameters for each embedding method and classification model and by leveraging different canonical forms of the SMILES formulas in the datasets. All of the unsupervised methods were trained on the 40 million compound dataset retrieved from ZINC, whereas the supervised methods were trained using each of the five labeled datasets described previously. We hereby describe the overall aspects of each method, including their neural-based architectures and the main characteristics of the obtained molecular representations. We provide further details on each model’s parameterization and training in the Supporting Information.

Unsupervised Methods

*SMILESVec*³³ is an unsupervised method for learning molecular representations from SMILES formulas, initially intended to represent proteins based on the combination of their ligands’ vectors. The architecture of the model consists of an autoencoder based on a feed-forward neural network, as proposed by Mikolov et al.³⁸. According to the original paper, we first tokenized the SMILES formulas into overlapping substrings of eight characters and compiled a vocabulary set with all the tokens in the training set. Considering the long-term dependencies that are often present in the SMILES sequences, such as branches or stereochemistry information, and that the eight-gram tokenization might limit the ability of the model to learn from them, we employed two different canonicalization processes on the ZINC training data. We thus obtained two different training sets for this method. On the one hand, we employed RDKit canonical SMILES formulas,⁴⁷ whereas, on the other hand, we tested *DeepSMILES* canonical formulas,⁴⁸ which are built by eliminating cycles in the molecular graph in order to reduce long-term dependencies in the sequences. *DeepSMILES* has also been employed by the authors who proposed *SMILESVec* on a follow-up study,³⁷ which

showed improved performance over the results obtained with traditional SMILES formulas.

As proposed by the authors of the *SMILESVec* architecture, a Skip-gram *word2vec* model³⁸ is used, where the size of the embeddings is determined by the number of nodes in its hidden layer. We trained two different models for each canonicalization technique mentioned above, accounting for two different embedding sizes: 100 and 300. The embedding size used in the original paper was 100. Additionally, we decided to test 300-dimensional embeddings to compare *SMILESVec* against higher-dimensional embeddings obtained by other methods tested in this paper. As performed by Öztürk et al.³³ in the original paper, the models were trained for 20 epochs, and the final molecular representations were obtained by computing the average of the learned vectors for each token in the SMILES formulas.

*Mol2Vec*¹² is also an unsupervised molecular embedding method based on *word2vec*.³⁸ The architecture of the model reported by the authors consists of a Skip-gram *word2vec* model, where the embedding size matches the size of the hidden layer of the autoencoder. Following the preprocessing steps indicated by Jaeger et al.¹² in their original paper, we tokenized the RDKit canonical SMILES formulas in the ZINC dataset into sequences of chemical words obtained by employing an adaptation of the Morgan algorithm, based on the graph traversal employed for computing ECFPs.²⁴ We decided not to employ *DeepSMILES* canonical SMILES to train this method since the Morgan algorithm cannot reconstruct the molecular graph from them. We compiled a vocabulary set including all chemical words obtained from the ZINC training dataset and trained two models for 5 epochs each, with embedding sizes 100 and 300, respectively, following the reference paper. Finally, we obtained the molecular embeddings by computing the sum of the learned vectors of all tokens in each molecule, as reported by the authors of the method.

The third and last unsupervised method we reproduced is *Seq2Seq*,³⁴ an embedding model consisting of an RNN-based autoencoder. The SMILES formulas in the ZINC training set were canonicalized to both RDKit and *DeepSMILES* canonical SMILES. While RDKit canonical SMILES were used in the reference paper, we decided to additionally em-

ploy *DeepSMILES* canonical formulas aiming to reduce the long-term dependencies in the SMILES sequences and thus test whether this contributed to the learning process of the method. The sequences in both datasets were tokenized by splitting the SMILES strings into separate characters and padded to match the length of the longest sequence in the dataset, as performed in the reference paper. According to Xu et al.³⁴, the architecture of the model consists of a multi-layer bidirectional LSTM autoencoder, and the learned embeddings are obtained by concatenating the hidden states of the trained model. Thus, their size is determined by the number of hidden units and the autoencoder layers. We trained two different models for each of the canonical forms of SMILES strings, obtaining 100-dimensional and 384-dimensional embeddings. Size 384 was the default embedding size reported by the authors of the method, and we also tested size 100 to account for a fair comparison to *SMILESVec* and *Mol2Vec*. We provide a summary of the molecular embeddings we obtained after training all the mentioned variants of the unsupervised methods in Table 2.

Table 2: Summary of all unsupervised methods and the outcoming embeddings. The column *Denomination* denotes the name we employ to refer to each of the learned embeddings throughout this paper. The denominations marked with an asterisk (*) correspond to the embeddings we decided to experiment with in addition to the ones proposed in the reference papers.

Method	Canonicalization	Embedding Size	Denomination
SMILESVec	RDKit	100	SMILESVec_100
		300	SMILESVec_300*
	DeepSMILES	100	Deep_SMILESVec_100
		300	Deep_SMILESVec_300*
Mol2Vec	RDKit	100	Mol2Vec_100
		300	Mol2Vec_300
Seq2Seq	RDKit	100	Seq2Seq_100*
		384	Seq2Seq_384
	DeepSMILES	100	Deep_Seq2seq_100*
		384	Deep_Seq2seq_384*

Supervised Methods

*PaccMann*¹¹ is a supervised method based on a set of multi-modal neural-based encoders that learn from both SMILES formulas and gene expression information, initially designed for predicting anticancer compound sensitivity. In particular, we reproduced the *Self-attention (SA)* encoder proposed by the authors, which they reported that yields the best results of all encoders proposed. Unlike the reference paper, we did not employ gene expression information in the training phase and instead trained the self-attentive encoder using only RDKit canonical SMILES formulas. In order to attain such a model, we adapted the source code provided by Oskooei et al.¹¹^{vii}. According to the reference paper, the SMILES formulas were tokenized following an algorithm⁴⁹ that consists of separating the SMILES formulas into characters and performing a basic filtering step. After such tokenization, each sequence was padded to match the longest sequence in the dataset.

As proposed by the reference paper, the architecture of *PaccMann* consists of an input layer by which the tokenized SMILES formulas are fed to the model. Next, a sinusoidal positional encoding function⁹ can be applied to these inputs. Afterward, such inputs are fed to a single-headed self-attention layer, whose implementation details are in the reference paper.¹¹ Finally, and according to the architecture originally proposed by the authors, the outcome of such self-attentive layer is fed to a shallow feed-forward neural network for property prediction. The learned molecular embeddings were extracted from the output of the self-attention layer, and their size is computed as the product between the number of hidden units in the self-attention layer and the length of the input sequence. Consequently, the embedding size is different for each of the five labeled datasets on which this method was trained. A summary of the embedding dimensionality for each labeled dataset is provided in Table 3.

The second supervised method we include in this paper is *SA-BiLSTM*, by Zheng et al.¹⁰. *SA-BiLSTM* consists of a self-attentive model combined with a bidirectional RNN using

^{vii}<https://github.com/drugilsberg/paccmann>.

LSTM nodes and followed by a shallow feed-forward neural network for property prediction. According to the reference paper, we trained this model using *Mol2Vec* embeddings¹² as input data, which were computed for the five labeled datasets described previously and using a pre-trained model provided by Jaeger et al.¹². The SMILES formulas were canonicalized using RDKit before computing the embeddings. Unlike the other methods tested in this paper, the authors of *SA-BiLSTM* have not provided the source code or an installable package for their method. Therefore, we reproduced the model from the equations and details provided in their paper.

According to the authors, the architecture of *SA-BiLSTM* consists of an input layer fed with the *Mol2Vec* embeddings and followed by a single-layer bidirectional LSTM-based RNN. The output of such a layer is then passed to a multi-head self-attention layer, which yields the final self-attentive embeddings of the molecules. Such embeddings are fed to a shallow feed-forward neural network for target prediction, which appears to be a single fully-connected layer. Further details about this model can be found in the reference paper.¹⁰ The self-attentive embeddings obtained from this model consist of a set of r vectors of size $2u$, where r is the number of attention heads and u is the number of hidden units in the LSTM layer (the factor of 2 is because the RNN is bidirectional). According to the reference paper, these embeddings (the r vectors) can be analyzed separately. However, since we wanted to use the learned information from all the attention heads for a classification task, we decided to concatenate them for the subsequent classification step. Thus the resulting embeddings consist of vectors of size $r \times 2u$. Because of the fitting process, and similarly to the case of *PaccMann*, the size of the embedding varies for each of the five labeled datasets used to train *SA-BiLSTM*. A summary of the *SA-BiLSTM* embedding dimensionality for each labeled dataset is provided in Table 3.

Table 3: Summary of all supervised methods and the outcoming embedding sizes.

Method/Denomination	Dataset	Embedding Size
PaccMann	SR-ARE	12000
	SR-MMP	24000
	SR-ATAD5	24000
	HIV	24200
	PCBA-686978	6976
SA-BiLSTM	SR-ARE	2560
	SR-MMP	1920
	SR-ATAD5	1280
	HIV	2560
	PCBA-686978	1280

Experimental Design

In this section, we give an overview of the experimental workflow we conducted to obtain from and evaluate the molecular embeddings for each of the reviewed methods. In an effort to achieve reproducibility and fairness in comparison, we provide a thorough explanation of all the steps involved in the training phase of each method and the subsequent embedding extraction for each labeled dataset. We also include a detailed description of the follow-up evaluation process, which consists of different classifiers that were trained with the different molecular embeddings. We also list the metrics that we used to evaluate all intermediate and final results. A summary of the workflow can be found in Figure 2.

Training and Embedding Extraction

The first step of the experimental setup consisted of training a model for each of the reviewed embedding methods. The training phase of the unsupervised methods (*SMILESVec*, *Mol2Vec* and *Seq2Seq*) was simpler than that of the supervised methods since the training dataset is unlabeled, and thus no early stopping criteria to avoid overfitting is needed. We trained each method for the time or epochs specified in each reference paper and following the hyperparameterization indicated in them. We obtained ten unsupervised embeddings for each combination of reviewed unsupervised method, embedding size and SMILES canonical-

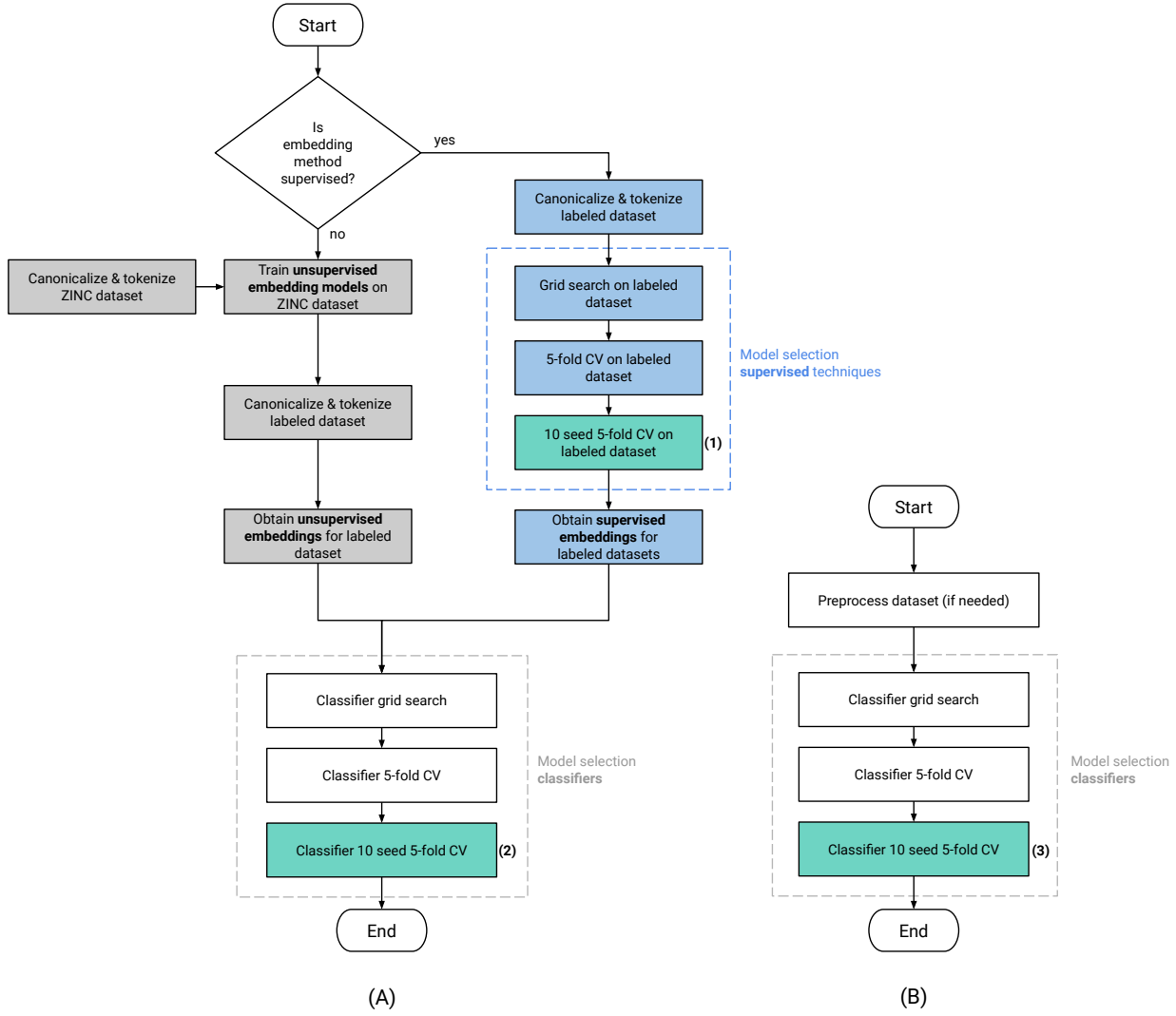


Figure 2: Overview of the experimental workflow: (A) corresponds to the workflow for embedding-based representations, whereas (B) depicts the workflow for traditional molecular representations, in accordance with Figure 1. The diagram cells in grey correspond to the experiments on the unsupervised embedding techniques, whereas the diagram cells in blue correspond to the experiments on the supervised techniques. The three final cells correspond to the QSAR modeling stage. The cells in green indicate the reported classification results: (1) the *fitting* results; i.e., the classification results obtained from the supervised embedding methods as a result of their training process (2) the classification results obtained from the baseline classifiers trained using either supervised or unsupervised embeddings. (3) the classification results obtained from the baseline classifiers trained using traditional molecular representations.

ization of the ZINC training dataset, as summarized in Table 2. Finally, we extracted the molecular embeddings for each of the five labeled datasets from the ten embedding models, whose SMILES formulas were previously tokenized as required by each proposed approach.

Regarding the supervised methods (*PaccMann* and *SA-BiLSTM*), we conducted a broader range of experiments during their training stage compared to the experiments on the unsupervised methods. As we have argued in previous sections of this paper, our goal was to attain embedding models whose differences at testing time could not be attributed solely to variance in the separation of data for training, in the initialization of the weights of the model or to nuances in the chosen hyperparameters. For this reason, we designed a training stage of the supervised embedding methods as follows:

1. We filtered and tokenized the compounds of the five labeled datasets according to the requirements of each of the supervised methods.
2. We performed a model selection consisting of two steps. First, we conducted a hyperparameter grid search that consisted of an exploratory search for the best performing hyperparameter combination for each method. For both methods, the ranges of hyperparameter values were defined so that they include those tested in the reference papers^{10,11} and expanded to other values that could have a positive impact on the training phase. As a result of this step, we selected the combinations of hyperparameters that yielded top results on each labeled dataset:
 - In the case of the *PaccMann*, we varied the number of hidden units (i.e. 16, 50 and 100) and the attention depth value (i.e. 20, 50, 100 and 256) used in the self-attention layer. We also tested different architectures for the feed-forward neural network used for property prediction, and varied the number of hidden units (i.e. [512, 256, 64, 16], [100, 50, 20, 5], [150, 50, 10] and [100, 20, 5]) and the activation functions (i.e. *ReLU* and *sigmoid*)⁵⁰ in the dense layers. We trained with and without a sinusoidal positional encoding function applied to the inputs,⁹ and

with and without a weighed loss function based on the imbalance in each class.⁵¹

We also varied regularization hyperparameters such as dropout coefficients per layer (i.e. 0.5, 0.25 and 0.15) and *lambda* values (i.e. 0.0001, 0.005 and 0.001) for L2-regularization.⁵² The learning rate was fixed to 0.001, and we used Adam optimizer.⁵³ We used a minibatch size of 512 for the small dataset (i.e. *SR-ARE*, *SR-MMP*, *SR-ATAD5*) and a minibatch size of 2048 for the large datasets (i.e. *HIV*, *PCBA-686978*). As a result of the grid search of *PaccMann*, we tested a total of 175 different combinations of hyperparameters for each labeled dataset.

- In the case of *SA-BiLSTM*, we explored a narrower range of hyperparameter values than those of *PaccMann*. Because of the time that each run of this method took to train, we decided to focus on the hyperparameters tested by the authors in the original paper. We varied the number of attention heads (i.e. 5, 10, 15 and 18) and the attention depth value (i.e. 10, 20, 50 and 100) in the self-attention layer, as well as the number of hidden units in the Bi-LSTM RNN (i.e. 64 and 128). Following the values indicated in the reference paper, we used a minibatch size of 64 for all datasets and used a gradient clipping coefficient of 0.3. The dropout coefficient per layer was set to 0.2 and the λ value for L2-regularization⁵² to 0.01. The models were trained for a maximum of 1000 epochs, as per the reference paper. In addition, we decided to run a grid search by applying the class ratio information of the datasets to the training phase in order to compensate class imbalance. As a result of the grid search stage of *SA-BiLSTM*, we tested a total of 64 different combinations of hyperparameters for each labeled dataset.

3. During the second step of the model selection stage, each of the hyperparameter combinations selected in the previous step was further tested on a stratified five-fold cross-validation process. The purpose of this stage was to confirm that the seemingly good results found during the grid search were not imputable only to the data partition used during that process. As a result, we selected a single combination of hyperparameters

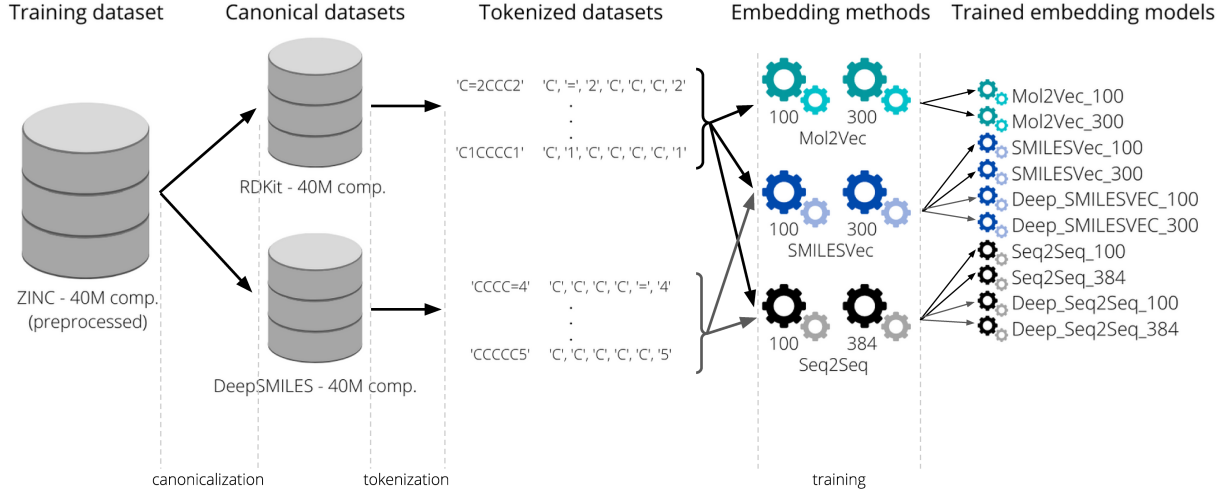
for each labeled dataset based on the average results of the five-fold cross-validation process.

4. We performed a replication analysis consisting of training ten trials of the model selected during the previous steps. We ran 10 trials of five-fold cross-validation using the same folds as before, each trial using a different random seed for weights initialization. This step was carried out to rule out any artifacts in the results that might have been caused by a particularly favorable random initialization of the weights of the embedding models in the previous steps. From this step, we obtained the classification results obtained from the inherent training process of the supervised embedding methods, which we refer to as *fitting* results.
5. Since a single embedding model was needed to extract the supervised embeddings, we trained an embedding model using a stratified data partition (80% train – 20% internal validation for early stopping). Finally, we extracted the molecular representations for each labeled dataset from these embedding models.

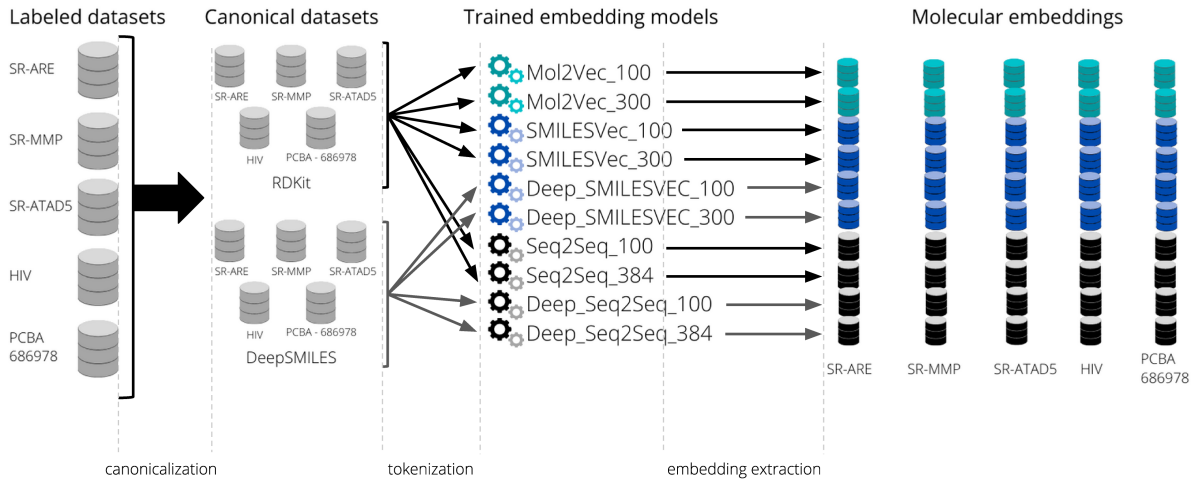
In addition to Figure 2, which summarizes the whole experimental workflow of our paper, we provide a more detailed graphical summary of the training stage of the unsupervised and supervised methods in Figures 3 and 4, respectively.

Evaluation of the Molecular Embeddings

In this paper, we aimed at comparing the usefulness of different learned molecular representations in the context of QSAR modeling. For this purpose, we conducted a comprehensive evaluation of the methods under study through five classification tasks, defined by the five labeled datasets described in Table 1. We obtained a total of ten combinations of unsupervised molecular embeddings and two combinations of supervised molecular embeddings per labeled dataset, as shown in Figures 3 and 4. Besides, we computed three traditional molecular representations for each of the labeled datasets: a 1024-bit ECFP fingerprint using



(a) Unsupervised training using 40 million compounds from ZINC dataset



(b) Embedding extraction

Figure 3: Training and embedding extraction from unsupervised methods: (a) The ZINC dataset was pre-processed and canonicalized following two different canonicalization procedures. The compounds in the two canonical datasets were tokenized as required by each of the unsupervised techniques, and then each unsupervised embedding model was trained. (b) The five labeled datasets were canonicalized and tokenized according to the requirements of each method. Afterward, molecular embeddings were obtained for the five labeled datasets from each of the unsupervised embedding models trained in the previous step.

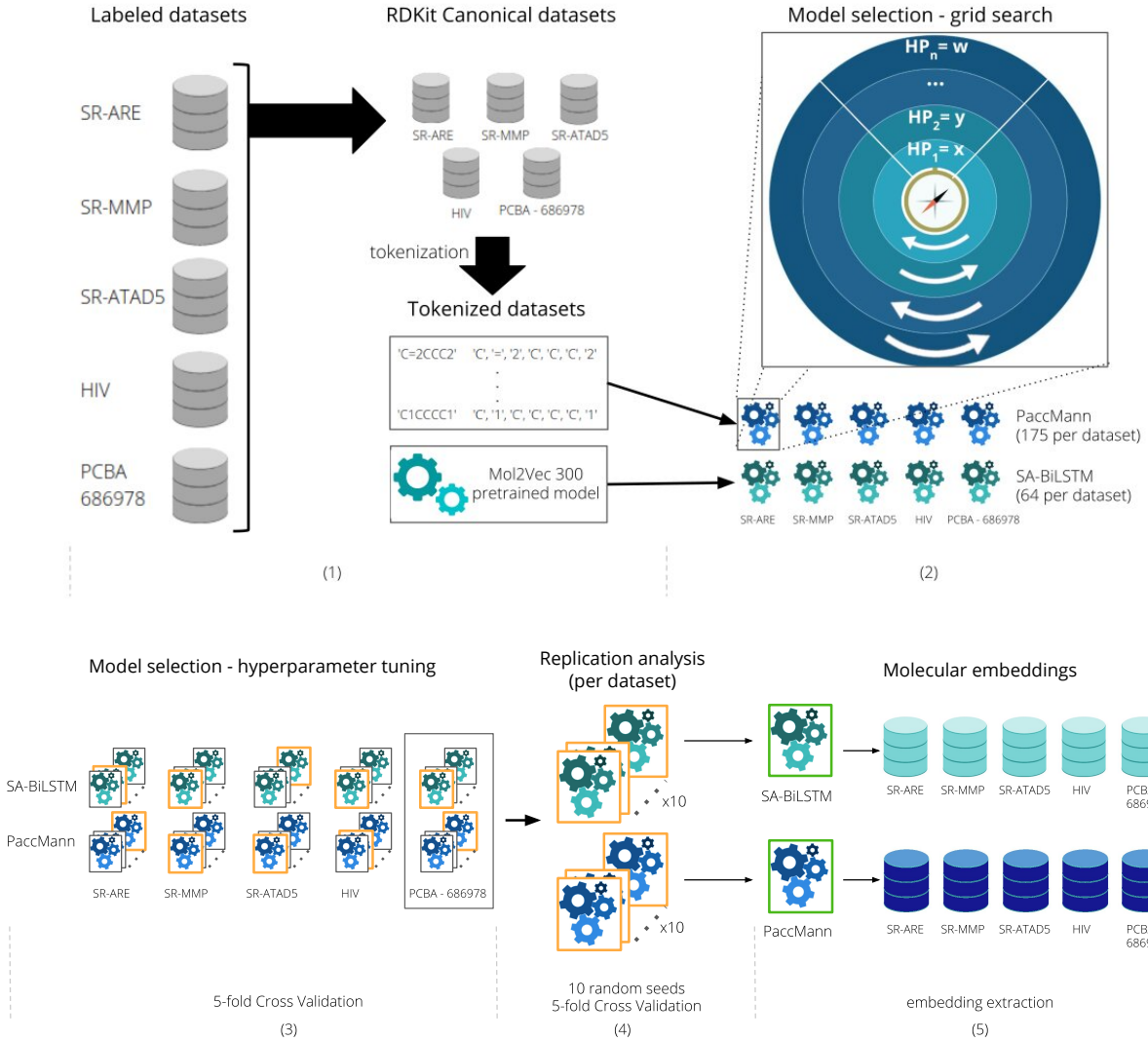


Figure 4: Training and embedding extraction from supervised methods: (1) The compounds in the five labeled datasets were preprocessed and tokenized. (2) First step of model selection on each labeled dataset: an exploratory grid search for the best performing hyperparameter combination for each method. As a result, a subset of hyperparameter combinations was chosen for each labeled dataset. (3) Second step of the model selection stage: each hyperparameter combination in the subset was tested on a five-fold cross-validation process. As a result, only one combination of hyperparameters was selected for each labeled dataset (highlighted in yellow). (4) Ten trials of the selected combination using different random seeds on five-fold cross-validation were trained. (5) An embedding model was trained using a stratified data partition and the embeddings for the five labeled datasets were obtained from such model.

RDKit⁴⁷ using radius $r = 2$, a 166-bit MACCS keys fingerprint also computed with RDKit, and a vector of molecular descriptors computed using Mordred.⁵⁴ We computed 0D, 1D and 2D descriptors for all datasets and discarded those having more than 5% of *Nan* entries. The final number of molecular descriptors varies for each labeled dataset: 1018 for SR-ARE, 1016 for SR-MMP and SR-ATAD5, 1150 for HIV and 1428 for PCBA-686978. All three representations were computed from RDKit canonical SMILES formulas.

In summary, we computed a total of 15 ($10 + 2 + 3$) representations for each dataset that we then used to train four different classifiers. In order to account for a fair comparison among all representations and molecular embeddings, we repeated the following steps for each representation:

1. We built and trained a Naïve Bayes classifier (NB), a Support Vector Machine (SVM) with an RBF kernel,⁵⁵ a Random Forest classifier (RF) and a shallow feed-forward neural network (FFNN). We used the Complement Naïve Bayes, SVM and RF implementations provided by Scikit-learn,⁵⁶ whereas the FFNNs were built and trained using Keras⁵⁷ and Tensorflow.⁵⁸ In the case of the three smallest labeled datasets (*SR-ARE*, *SR-MMP* and *SR-ATAD5*), we trained single SVMs. In contrast, for the two largest labeled datasets (*HIV* and *PCBA-686978*), for which training a standard non-linear kernel SVM on all compounds would have taken an inadmissible amount of time, we decided to employ the Scikit-learn implementation of a bagging classifier of ten SVMs, each trained on a stratified sample consisting of one-tenth of the dataset.

We conducted a grid search using a stratified data partition. In the case of the SVMs, we varied the regularization coefficient $c \in \{0.01, 0.05, 0.1, 0.25, 0.5, 1, 5, 10, 20\}$, and for the RF classifier we varied the maximum depth of the tree $md \in \{2, 3, 5, 8, 10, 20\}$. For the FFNNs, we varied the number of nodes in each layer (i.e. [150, 50, 10], [100, 50, 10] and [100, 20, 5]), the L2-regularization hyperparameter $\lambda \in \{0.0001, 0.005, 0.001\}$, the minibatch size $b \in \{64, 128, 256, 512\}$, the activation function used in the hidden layers (i.e. ReLU and *tanh*) and the early-stopping *patience* coefficient $p \in \{70, 100, 200, 500\}$.

We also tested different learning rates $\alpha \in \{0.00001, 0.0001, 0.001\}$. Further details about the parameterization of these classifiers are provided in the Supporting Information.

2. We selected the best parameterizations of each method and ran a five-fold cross-validation training procedure. Similar to the training stage of the supervised embedding methods, the goal of this phase was to confirm that the results found during the grid search were not bound to the specific data partition used in the previous step.
3. We selected the single best parameterization based on the results obtained during the five-fold cross-validation stage. Afterward, we ran ten trials of five-fold cross-validation using the same folds as before and using a different random seed for each run. This step was carried out for the stochastic classification methods (i.e., RF, FFNN and ensembles of SVMs). In this way, we ensured that the obtained classification results were not just due to a lucky random initialization of the weights of the classification models.

During every stage of the training process we used the same folds for each labeled dataset in every single stage of the experiments. Thus, we can reduce the variance associated with random data partition. In all cases, we measured the average results of the five validation folds and their 95% confidence intervals.

Results and Discussion

This section discusses the results obtained for the five classification tasks defined by each of the labeled datasets. We compare the results using all the molecular embedding techniques on the four classifiers described in the previous section. In addition, we report the classification results obtained by the supervised methods during the embedding learning stage—i.e., the *fitting* results. The classification results obtained from other traditional molecular representations (i.e. *molecular descriptors*, *ECFPs* and *MACCs keys*) were considered baselines.

Throughout all stages of our experiments, including model selection, we measured the performance of our models using eight different metrics: *Sensitivity (Sn)*, *Specificity (Sp)*, *Precision*, *Accuracy (Acc)*, *Balanced Accuracy (BA)*, F_1 score, H_1 score and *Area Under the ROC Curve (AUC)*. *BA* is computed as the arithmetic mean of *Sn* and *Sp* and F_1 score is computed as the harmonic mean of *Sn* and *Precision*. To avoid overriding the notation for F_1 score, we hereby redefine the harmonic mean of *Sn* and *Sp* as H_1 score, which is often called F_1 or *F* score in the literature.⁵⁹ We prioritized F_1 score and H_1 score to make hyperparameter selections, since they are suitable metrics in contexts of highly imbalanced datasets (such as in the case of HIV and SR-ATAD5) in contrast to metrics like *Acc*.^{59,60} All the results obtained for each step of our experimental workflow in all five datasets can be found in the Supporting Information.

In order to assess the statistical significance of the results, we conducted a series of tests through which we compared the F_1 score results obtained by the different molecular representations and QSAR models on each dataset. We first conducted a two-way ANOVA where *molecular representation* and *classifier choice* were considered the two independent variables. Upon eventually finding that the molecular representations had significant differences on the results under study, we conducted a *post-hoc* pairwise Tukey test⁶¹ with a global confidence level of 95%. We present the results of this test on FFNN classifiers in Figure 6. Full tables with the results of these statistical tests can be found in the Supporting Information.

Our first research question (Q1) aimed at determining whether learned molecular representations were suitable for QSAR modeling and, in particular, whether they could outperform traditional molecular representations. In order to answer this question, we compared the results obtained using the traditional molecular representations—*molecular descriptors*, *ECFPs* and *MACCS keys*—to the results obtained using learned molecular embeddings, considering both supervised and unsupervised methods. After conducting the two-way ANOVA test, which provided statistical evidence that the results obtained among the representations were significantly different, we proceeded to compare the fifteen representations under study,

one classifier at a time, using a pairwise Tukey test.

As it can be seen in Figure 5, for NB, RF and SVM classifiers, traditional molecular representations were among the top-performing representations for all datasets, yielding significantly better results than most learned embeddings. In the case of the imbalanced datasets—*SR-ATAD5* and *HIV*—, *ECFP* was significantly better than other representations in NB-based classifiers and among the top-performing representation for the other classifiers, as shown in Figures 5 (c) and (d). *MACCS keys* and *molecular descriptors* also yielded significantly better results than learned embeddings in most datasets and classifiers. In the case of *PCBA-686978* (Figure 5 (e)), the best results were obtained by traditional representations in all classifiers except for FFNN. Another interesting finding is that there were no significant differences among the results obtained using the three traditional representations.

In the case of FFNN, the best results were generally obtained using *SA-BiLSTM*: this was observed for datasets *SR-ARE*, *SR-MMP* and *SR-ATAD5*. For dataset *HIV*, the best FFNN results were obtained by *ECFP*, showing a significant difference to all learned embeddings, whereas *Mol2Vec_300* yielded the best results on FFNN for dataset *PCBA-686978*, which is the largest labeled dataset comprising 302175 compounds. In all cases, these results were significantly better than those obtained using other learned embeddings, as shown in Figure 6.

In general, the results using unsupervised embeddings did not match the results obtained by the traditional representations, except for *Mol2Vec* embeddings in FFNN classifiers. The statistical tests showed in all cases that the differences among these results were significant.

Our second research question (Q2) intended to determine whether supervised molecular embeddings could surpass unsupervised molecular embeddings in terms of classification performance. In this case, we conducted a two-way ANOVA test among all learned molecular embeddings, which once again provided statistical evidence supporting the fact that the results obtained using different embedding methods were significantly different. Afterward, we

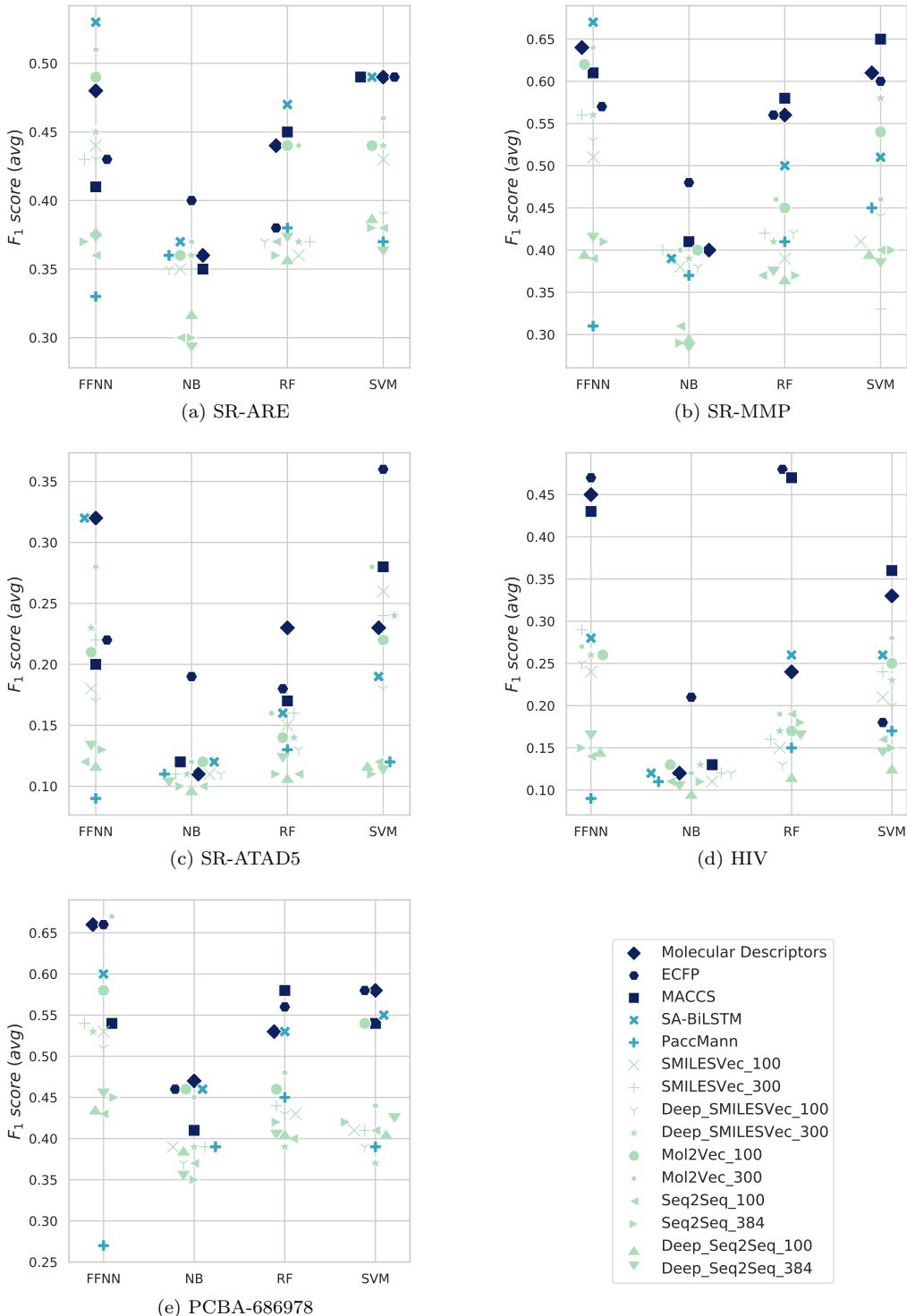


Figure 5: F_1 scores for the five labeled datasets. Dark blue denotes traditional representations, light blue shows supervised embeddings, and green denotes unsupervised embeddings. Random horizontal jitter is applied to the markers to avoid overlap. Traditional representations attained the best performances in most cases, matched or followed by *SA-BiLSTM* and *Mol2Vec* embeddings.

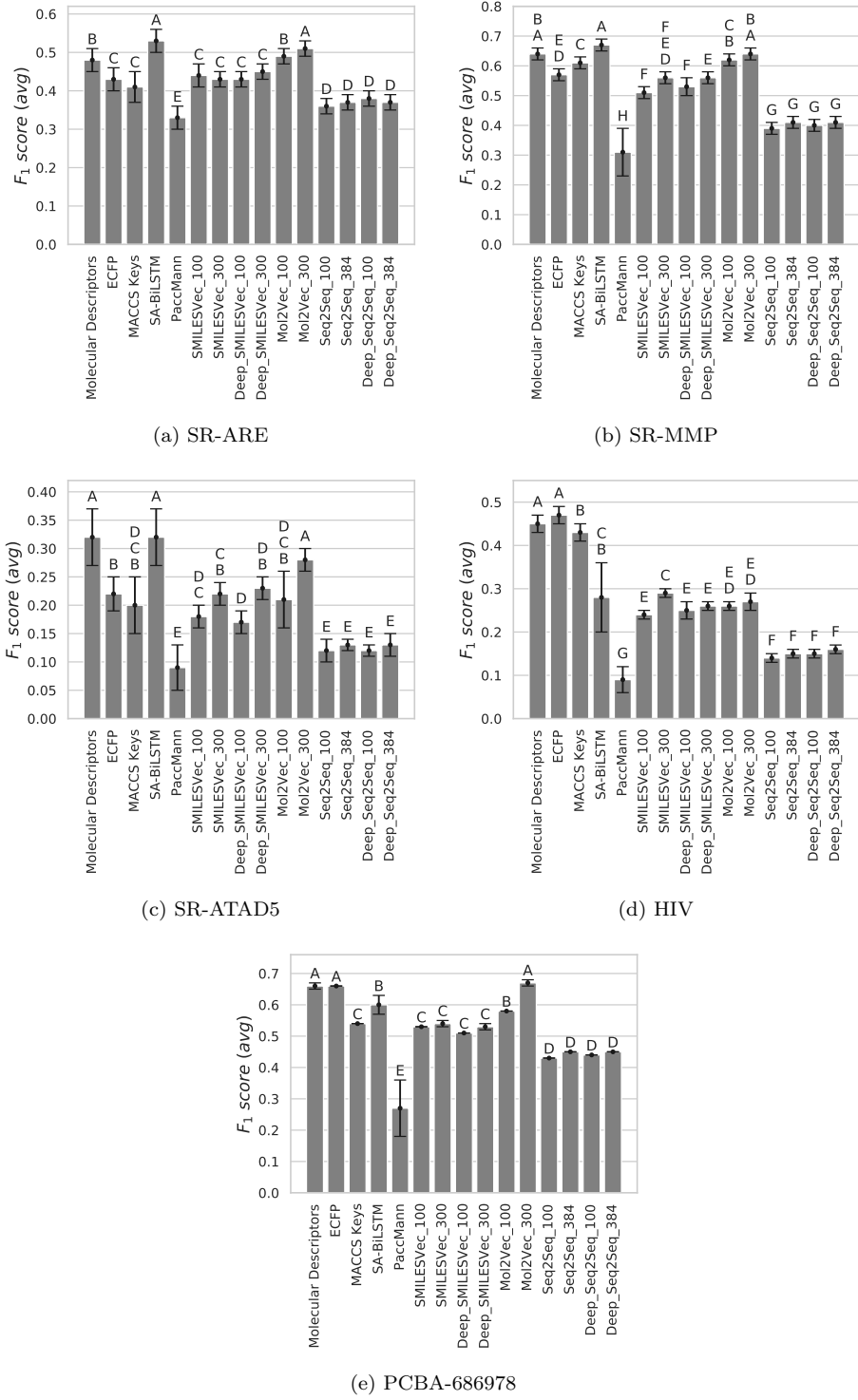


Figure 6: F_1 score obtained by all molecular representations in the FFNN classifier. Means with the same letter are not significantly different, according to the pairwise Tukey test. The results obtained using *Seq2Seq* embeddings are not statistically different in any of the datasets. *Mol2Vec* tends to show different results depending on their embedding size and are not different to *SA-BiLSTM* embeddings of traditional representations.

performed a pairwise Tukey test to compare the results obtained in each classifier using the supervised embeddings against the unsupervised embeddings.

After such analysis, and as it is shown by Figure 5, we observed that the results obtained using the supervised representation *SA-BiLSTM* were generally significantly better than the results obtained employing unsupervised embeddings, especially in the case of the balanced datasets (*SR-ARE*, *SR-MMP* and *PCBA-686978*). This observation, however, did not hold in the case of the NB-based classifiers, for which no significant differences among classification results were observed in any of the datasets. In the case of datasets *SR-ATAD5*, *HIV* and *PCBA-686978*, *SA-BiLSTM* attained similar results to those obtained by *Mol2Vec_100* and *Mol2Vec_300* in all classifiers except RF, which might be related to the fact that *SA-BiLSTM* is trained using a form of *Mol2Vec* embeddings.

In the case of *PaccMann*, the results did not show significant differences to the results obtained employing any of the unsupervised molecular embeddings in the majority of the cases, except for FFNN-based classifiers, where the results are poor and significantly different from all other representations. This can be observed in Figures 5 and 6 as well. This phenomenon could be explained by the inherent high dimensionality in *PaccMann* embeddings—ranging from 6976 to 24,200 dimensions, as shown in Table 3—, which is often a cause of traditional classifiers having difficulties in learning patterns from the data and, consequently, of a low classification performance.^{62,63} It is worth noticing that the original *PaccMann* embedding model proposed by Oskooei et al.¹¹ was developed as a multimodal encoder for anticancer compound sensitivity prediction. Therefore, the difference in the performance exhibited by the encoder in the reference paper and our results could also be attributed to not having employed gene expression information in the training procedure.

When analyzing the *fitting* results of the supervised embedding methods—i.e., obtained as a result of the training phase followed in order to obtain the molecular embeddings—, as it can be seen in Figure 7, *SA-BiLSTM* was once again significantly better than *PaccMann* for all five datasets. However, it is worth noticing that the *fitting* results obtained by *PaccMann*

were, in the case of datasets *PCBA-686978* and *SR-MMP*, significantly better than those obtained by such embeddings with the other classifiers (NB, SVM, RF and FFNN). In the case of *SA-BiLSTM*, the *fitting* results were surpassed by at least one other classification technique in all datasets except for *PCBA-686978*. However, this issue could be due to the number of nodes in the layers dedicated to property prediction in the *SA-BiLSTM* model.

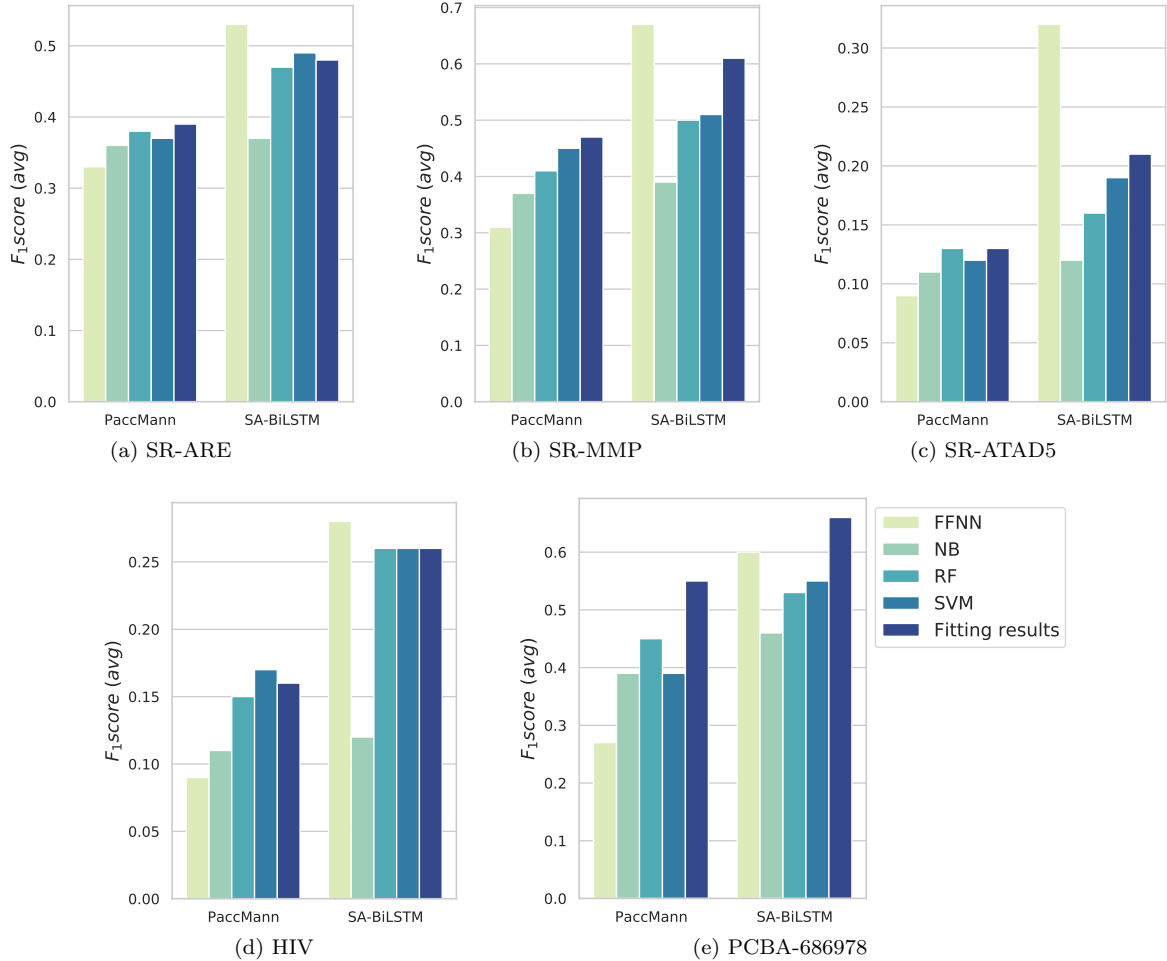


Figure 7: F_1 scores for the five labeled datasets using the supervised embeddings. *SA-BiLSTM* obtained top results among the supervised embeddings, especially on FFNN. While *PaccMann* results were significantly worse than those obtained by *SA-BiLSTM*, its *fitting* results—i.e., the classification results obtained from training the embedding model—were usually better than those obtained on other classifiers.

Our third research question (Q3) aimed to determine whether the canonical form of the SMILES formulas used to train the embedding methods or the final embedding sizes

had a significant impact on the classification performance of QSAR models. To answer this question, we analyzed the three unsupervised embedding techniques separately, whose results can also be found in Figure 5. We conducted separate two-way ANOVA tests and the corresponding pairwise Tukey tests to compare the results obtained by the following groups of molecular embeddings:

- *SMILESVec_100, SMILESVec_300, Deep_SMILESVec_100* and *Deep_SMILESVec_300*: No significant differences were observed among the results in any of the five datasets while using different classification techniques, except for SVM in the case of the balanced datasets (*SR-ARE*, *SR-MMP* and *PCBA-686978*), where all results were significantly different. We observed that the results of *SMILESVec_300* and *Deep_SMILESVec_300* tended to be better than those obtained by *SMILESVEC_100* and *Deep_SMILESVec_100* when using FFNN for building the QSAR models; such differences, however, were statistically significant only for datasets *SR-MMP* and *SR-ATAD5*, as it can be seen in Figures 5 and 6.
- *Mol2Vec_100* and *Mol2Vec_300*: The results obtained were significantly different when changing the size of the embedding from 100 to 300 throughout the five datasets and, as it happened in the case of *SMILESVec*, 300-dimension embeddings outperformed 100-dimension embeddings. This phenomenon was observed in all classifiers except NB, which, as discussed previously, yielded similar results on all molecular representations.
- *Seq2Seq_100, Seq2Seq_384, Deep_Seq2Seq_100* and *Deep_Seq2Seq_384*: In the case of *Seq2Seq*, the changes in the canonicalization or the size of embeddings for this technique did not yield significantly different results in any of the five datasets.

Finally, we compared the results obtained by the top-performing molecular representations on each dataset to the results reported by the reference papers^{10,12} and state-of-the-art results for the datasets under study.^{44,64} These papers reported classification performance of their QSAR models in terms of *AUC* in the case of datasets *SR-ARE*, *SR-MMP*, *SR-ATAD5*

and *HIV*. In the case of dataset *PCBA-686978*, the original results were reported in terms of *Acc*,⁴⁴ even though such metric is not appropriate for imbalanced datasets.^{59,60} As shown in Table 4, the results obtained during our experiments always match or surpass the results obtained by the reference papers, which arguably shows that results appear to be sound and that the extensive model selection stage was important..

To analyze the stability of the representations, we present the classification results obtained by ten runs per molecular representation using FFNN classifiers, each using a different random initialization, in Figure 8. These results are expressed in terms of F_1 score and *AUC*, and they show the dispersion of the results of each molecular representation in terms of these two metrics. Interestingly, while *ECFP* attained the top results in terms of F_1 score for the majority of datasets, *SA-BiLSTM* matches or surpasses *ECFP* when analyzing the *AUC* results in all datasets except for *PCBA-686978*. As it can be seen in Table 4 and in Figure 8, *SA-BiLSTM* exhibits top *AUC* results on FFNN, often on pair with *molecular descriptors* and *Mol2Vec* embeddings. The dispersion of the results is often low within different runs with the same molecular representations, with exception of dataset *SR-ATAD5*, a highly imbalanced dataset comprising a relatively small number of compounds, which in turn makes it a relatively difficult classification task. It is worth noticing that, when looking at the results in terms of F_1 score, traditional representations surpassed the majority of unsupervised embeddings in the case of datasets *HIV* and *PCBA-686978*, which are the largest datasets. In the case of dataset *PCBA-686978*, the results obtained by *molecular descriptors* and *ECFP* were superior to all learned molecular embeddings for both metrics, with exception of *Mol2Vec_300* which also obtained the top results using FFNN. When analyzing other metrics, such as *Precision* and *Sp*, *ECFP* attained better results than *SA-BiLSTM* and *Mol2Vec_300*, which in turn explains the observed results in terms of F_1 score.

Based on our observations, we can conclude that, in general, learned molecular embeddings did not surpass the results obtained by traditional molecular representations. In particular, most of the unsupervised embeddings methods did not even match the results obtained

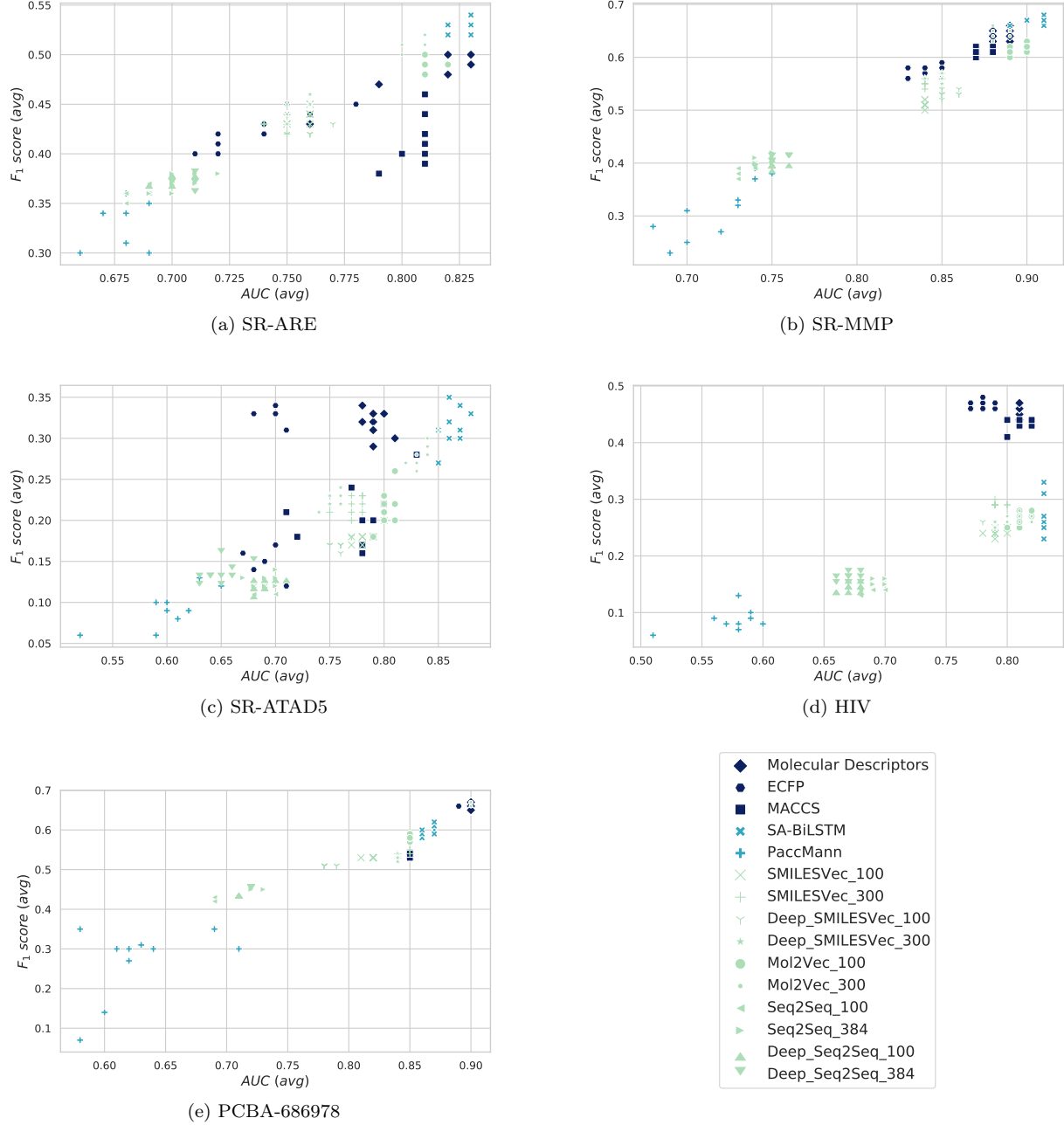


Figure 8: Results in terms of F_1 score and AUC for ten runs of FFNN classifiers, each using a different random initialization. *SA-BiLSTM* obtained the best results in most datasets, often matched by *molecular descriptors* or *Mol2Vec* embeddings. Traditional representations yielded better F_1 score results than *SA-BiLSTM* in the largest datasets (*HIV* and *PCBA-686978*).

Table 4: *AUC* and *Acc* results reported in the reference papers, in contrast to the top results obtained through our experimental workflow marked with an asterisk (*). The best results per dataset are highlighted in **bold**. *na* denotes that the authors of the reference paper do not provide the information. Our results always match or surpass the results obtained by the reference papers, thus ensuring their reproducibility and comparability to the state of the art. *SA-BiLSTM* surpasses *ECFP* when analyzing the *AUC* values, whereas *ECFP* yields superior *F*₁ score due to its higher *Precision*.

Representation	Classifier	AUC				Acc
		SR-ARE	SR-MMP	SR-ATAD5	HIV	
SA-BiLSTM ¹⁰	fitting	0.81 ± <i>na</i>	0.90 ± <i>na</i>	0.86 ± <i>na</i>	0.81 ± <i>na</i>	-
Mol2Vec ¹²	RF	0.83 ± 0.05	0.83 ± 0.05	0.83 ± 0.05	-	-
GCN ⁶⁴	fitting	0.83 ± 0.01	0.83 ± 0.01	0.83 ± 0.01	0.76 ± 0.02	-
SMILES-BERT ⁴⁴	fine-tuning	-	-	-	-	0.88 ± <i>na</i>
SA-BiLSTM (*)	FFNN	0.83 ± 0.02	0.91 ± 0.01	0.87 ± 0.02	0.83 ± 0.01	0.80 ± 0.04
Mol2Vec_300 (*)	FFNN	0.81 ± 0.01	0.88 ± 0.01	0.84 ± 0.01	0.81 ± 0.01	0.83 ± 0.00
ECFP (*)	FFNN	0.74 ± 0.02	0.84 ± 0.01	0.70 ± 0.04	0.78 ± 0.01	0.87 ± 0.00

by traditional molecular representations. Among the unsupervised embedding techniques, *Mol2Vec* tended to yield the best results, often performing significantly better than the results obtained using *SMILESVec* or *Seq2Seq*. This could be related to the preprocessing step that the SMILES formulas undergo before being fed to the *Mol2Vec* auto-encoder—which is based on the algorithm applied to obtain *ECFP* embeddings—in contrast to the simple tokenization steps applied to SMILES formulas in the case of the other two techniques. *Seq2Seq* obtained the lowest *F*₁ score results of all representations, especially in the case of imbalanced datasets *SR-ATAD5* and *HIV*.

In the case of supervised embeddings, on the one hand, *SA-BiLSTM* yielded the best results among the learned representations. However, they were often on par with those obtained using traditional molecular representations. On the other hand, *PaccMann* did not yield good results. As we discussed earlier in this section, the high dimensionality of *PaccMann* embeddings (as shown in Table 3) might be related to its poor performance in the majority of the classification tasks. Another possible reason for the significant difference between the results of the two supervised embedding techniques might be the way that self-attention is implemented, considering that *SA-BiLSTM* consists of a multi-head self-

attention model, whereas *PaccMann* is a single-head self-attention model.

Our results were designed to attain the best possible performance for each molecular representation. We conducted a wide range of experiments, varying the classification techniques, the dataset sizes and class imbalance scenarios. We also tested many different parameterizations and variations of the input data for each embedding method. The conclusions derived in this paper are presented after observing consistent and sound results throughout our analysis, which were also comparable to the results reported by the reference papers.^{10,12,44,64} This pattern of learned molecular representations matching the performance of traditional representations has also been noticed by other authors that experimented with learned molecular embeddings for QSAR modeling.¹²⁻¹⁶ However, such results were neither conclusive as they are not supported by any significance test nor conducted a systematic comparison where hyperparameters are tuned fairly. It also reminisces a common phenomenon in machine learning where simple modeling techniques are on pair with complex architectures.^{65,66} We believe that our experiments motivate a rethinking of molecular embedding techniques and the potential role of learned representations or meta-learning algorithms for QSAR modeling.

Although according to our experiments there is no evidence supporting that learned molecular embeddings yield better QSAR models than those obtained by traditional molecular representations, learned molecular embeddings might outperform traditional representations in other tasks in the spectrum of drug design and virtual screening, which opens a wide range of experimental possibilities and future work.^{2,3,23} While traditional representations are built or computed following a standard algorithm and looking at a single molecule at a time, learned embeddings can be computed from large sets of compounds, potentially yielding richer representations that could be suitable for molecular similarity analysis.^{2,67} Besides, techniques like self-attention might yield especially suitable embeddings for tasks like molecular substructure search, identifying most likely binding conformations or molecular docking,^{2,3,10} or for the identification of which substructures have an impact on the bioactivity profile of the compound.¹⁰

Conclusions

Many novel algorithms for learning molecular representations have been proposed in recent years, involving deep learning techniques. However, to the best of our knowledge, no systematic comparison of such techniques to traditional representations for QSAR modeling had been conducted. In this paper, we carried out an extensive comparison of five different techniques for learning molecular representations that consisted of over 20,000 trained models. We tested their suitability for QSAR modeling in five classification tasks. We evaluated different embedding sizes, SMILES canonicalizations and embedding methods and compared the results against those obtained using traditional molecular representations. Our experimental analysis shows no evidence of molecular embeddings surpassing molecular descriptors or fingerprints, which might indicate that traditional representations are as good at the task as molecular embeddings are. We also found that unsupervised molecular embeddings exhibited lower performance than supervised techniques in general.

Despite these findings, computer-aided drug design has numerous flourishing areas of research where there is room for experimentation with learned representations, such as *de novo* drug design, molecular docking or virtual screening,^{2,3} which makes this topic of utmost interest to the cheminformatics community. Contrary to deterring the computer-aided drug design community from using and developing new algorithms for learning molecular representations, we hope that the results observed in this paper can serve as an incentive to design new ways of using molecular embeddings to leverage their potential for different tasks in drug design.

Acknowledgement

This work was supported by CONICET research grant PIP 112-2017-0100829 (Argentina), ANPCyT research grant PICT-2019-03350 (Argentina), UNS research grant PGI 24/N042 (Argentina), NSERC Discovery grant (Canada), and by a Google LARA award (Google Latin

America Research Award 2020-2021). This research was partly supported by DeepSense^{viii}, ACENET^{ix}, Calcul Québec^x and Compute Canada^{xi}. Authors also thank Chris Whidden, Jason Newport and Lu Yang for their technical support with the DeepSense cluster.

Data and Software Availability

In order to ensure the reproducibility of our experimental workflow, all resources, materials and source code used in this paper are either properly cited or we have made them publicly available. The five labeled datasets used in this paper, both in *RDKit* and *DeepSMILES* canonical SMILES format, the computed molecular descriptors and fingerprints, the trained embedding models from which molecular embeddings can be extracted and the source code needed to reproduce our approach are all publicly available at a public repository^{xii}.

Supporting Information Available

Results obtained for each step of the experimental workflow in the five datasets along with details of model and classifier parameterization; results of statistical tests (two-way ANOVA and pairwise Tukey tests).

Conflict of Interest Disclosure

The authors declare no competing financial interest.

^{viii}<https://www.deepsense.ca/>.

^{ix}<https://www.ace-net.ca/>.

^x<https://www.calculquebec.ca/>.

^{xi}<https://www.computecanada.ca/>.

^{xii}https://csunseduar-my.sharepoint.com/:f/g/personal/virginia_sabando_cs_uns_edu_ar/EjUkG4X2A31EgJ0Aj0EjveYBMcoo08mKIpQoHquoQtdUhw

References

- (1) Cherkasov, A.; Muratov, E. N.; Fourches, D.; Varnek, A.; Baskin, I. I.; Cronin, M.; Dearden, J.; Gramatica, P.; Martin, Y. C.; Todeschini, R., et al. QSAR modeling: where have you been? Where are you going to? *Journal of Medicinal Chemistry* **2014**, *57*, 4977–5010.
- (2) Chuang, K. V.; Gunsalus, L. M.; Keiser, M. J. Learning Molecular Representations for Medicinal Chemistry: Miniperspective. *Journal of Medicinal Chemistry* **2020**, *63*, 8705–8722.
- (3) Elton, D. C.; Boukouvalas, Z.; Fuge, M. D.; Chung, P. W. Deep learning for molecular design—a review of the state of the art. *Molecular Systems Design & Engineering* **2019**, *4*, 828–849.
- (4) Chen, H.; Engkvist, O.; Wang, Y.; Olivecrona, M.; Blaschke, T. The rise of deep learning in drug discovery. *Drug Discovery Today* **2018**, *23*, 1241–1250.
- (5) Bouhedjar, K.; Boukelia, A.; Khorief Nacereddine, A.; Boucheham, A.; Belaidi, A.; Djerourou, A. A natural language processing approach based on embedding deep learning from heterogeneous compounds for quantitative structure–activity relationship modeling. *Chemical Biology & Drug Design* **2020**, *96*, 961–972.
- (6) David, L.; Thakkar, A.; Mercado, R.; Engkvist, O. Molecular representations in AI-driven drug discovery: a review and practical guide. *Journal of Cheminformatics* **2020**, *12*, 1–22.
- (7) Weininger, D. SMILES, a chemical language and information system. 1. Introduction to methodology and encoding rules. *Journal of Chemical Information and Computer Sciences* **1988**, *28*, 31–36.

(8) Wu, Z.; Pan, S.; Chen, F.; Long, G.; Zhang, C.; Philip, S. Y. A comprehensive survey on graph neural networks. *IEEE Transactions on Neural Networks and Learning Systems* **2020**, *32*, 950–957.

(9) Vaswani, A.; Shazeer, N.; Parmar, N.; Uszkoreit, J.; Jones, L.; Gomez, A. N.; Kaiser, L.; Polosukhin, I. Attention Is All You Need. *arXiv e-prints* **2017**, arXiv:1706.03762.

(10) Zheng, S.; Yan, X.; Yang, Y.; Xu, J. Identifying structure–property relationships through SMILES syntax analysis with self-attention mechanism. *Journal of Chemical Information and Modeling* **2019**, *59*, 914–923.

(11) Oskooei, A.; Born, J.; Manica, M.; Subramanian, V.; Sáez-Rodríguez, J.; Rodríguez Martínez, M. PaccMann: Prediction of anticancer compound sensitivity with multi-modal attention-based neural networks. *arXiv e-prints* **2018**, arXiv:1811.06802.

(12) Jaeger, S.; Fulle, S.; Turk, S. Mol2vec: unsupervised machine learning approach with chemical intuition. *Journal of Chemical Information and Modeling* **2018**, *58*, 27–35.

(13) Gómez-Bombarelli, R.; Wei, J. N.; Duvenaud, D.; Hernández-Lobato, J. M.; Sánchez-Lengeling, B.; Sheberla, D.; Aguilera-Iparraguirre, J.; Hirzel, T. D.; Adams, R. P.; Aspuru-Guzik, A. Automatic chemical design using a data-driven continuous representation of molecules. *ACS Central Science* **2018**, *4*, 268–276.

(14) Goh, G. B.; Siegel, C.; Vishnu, A.; Hodas, N. O.; Baker, N. Chemception: A Deep Neural Network with Minimal Chemistry Knowledge Matches the Performance of Expert-developed QSAR/QSPR Models. *arXiv e-prints* **2017**, arXiv:1706.06689.

(15) Yang, K.; Swanson, K.; Jin, W.; Coley, C.; Eiden, P.; Gao, H.; Guzman-Perez, A.; Hopper, T.; Kelley, B.; Mathea, M., et al. Analyzing learned molecular representations for property prediction. *Journal of Chemical Information and Modeling* **2019**, *59*, 3370–3388.

(16) Yang, K.; Swanson, K.; Jin, W.; Coley, C.; Eiden, P.; Gao, H.; Guzman-Perez, A.; Hopper, T.; Kelley, B.; Mathea, M.; Palmer, A.; Settels, V.; Jaakkola, T.; Jensen, K.; Barzilay, R. Correction to Analyzing Learned Molecular Representations for Property Prediction. *Journal of Chemical Information and Modeling* **2019**, *59*, 5304–5305, PMID: 31814400.

(17) Sterling, T.; Irwin, J. J. ZINC 15–ligand discovery for everyone. *Journal of Chemical Information and Modeling* **2015**, *55*, 2324–2337.

(18) Sabando, M. V.; Ulbrich, P.; Selzer, M.; Byška, J.; Mičan, J.; Ponzoni, I.; Soto, A. J.; Ganuza, M. L.; Kozlíková, B. ChemVA: Interactive Visual Analysis of Chemical Compound Similarity in Virtual Screening. *IEEE Transactions on Visualization and Computer Graphics* **2021**, *27*, 891–901.

(19) Martínez, M. J.; Ponzoni, I.; Díaz, M. F.; Vazquez, G. E.; Soto, A. J. Visual analytics in cheminformatics: user-supervised descriptor selection for QSAR methods. *Journal of Cheminformatics* **2015**, *7*, 1–17.

(20) Todeschini, R.; Consonni, V. *Molecular descriptors for chemoinformatics: volume I: alphabetical listing/volume II: appendices, references*; John Wiley & Sons, 2009; Vol. 41.

(21) Cereto-Massagué, A.; Ojeda, M. J.; Valls, C.; Mulero, M.; Garcia-Vallvé, S.; Pujadas, G. Molecular fingerprint similarity search in virtual screening. *Methods* **2015**, *71*, 58–63.

(22) Grisoni, F.; Consonni, V.; Todeschini, R. In *Computational Chemogenomics*; Brown, J., Ed.; Springer New York: New York, NY, 2018; pp 171–209.

(23) Schneider, G. Virtual screening: an endless staircase? *Nature Reviews Drug Discovery* **2010**, *9*, 273–276.

(24) Rogers, D.; Hahn, M. Extended-connectivity fingerprints. *Journal of Chemical Information and Modeling* **2010**, *50*, 742–754.

(25) Durant, J. L.; Leland, B. A.; Henry, D. R.; Nourse, J. G. Reoptimization of MDL keys for use in drug discovery. *Journal of Chemical Information and Computer Sciences* **2002**, *42*, 1273–1280.

(26) Seth, A.; Roy, K. QSAR modeling of algal low level toxicity values of different phenol and aniline derivatives using 2D descriptors. *Aquatic Toxicology* **2020**, *228*, 105627.

(27) Yang, L.; Wang, Y.; Chang, J.; Pan, Y.; Wei, R.; Li, J.; Wang, H. QSAR modeling the toxicity of pesticides against *Americamysis bahia*. *Chemosphere* **2020**, *258*, 127217.

(28) Gao, K.; Nguyen, D. D.; Sresht, V.; Mathiowitz, A. M.; Tu, M.; Wei, G.-W. Are 2D fingerprints still valuable for drug discovery? *Physical Chemistry Chemical Physics* **2020**, *22*, 8373–8390.

(29) Sabando, M. V.; Ponzoni, I.; Soto, A. J. Neural-based approaches to overcome feature selection and applicability domain in drug-related property prediction. *Applied Soft Computing* **2019**, *85*, 105777.

(30) Idakwo, G.; Luttrell IV, J.; Chen, M.; Hong, H.; Gong, P.; Zhang, C. A review of feature reduction methods for qsar-based toxicity prediction. *Advances in Computational Toxicology* **2019**, 119–139.

(31) Liu, S.; Furkan Demirel, M.; Liang, Y. N-Gram Graph: Simple Unsupervised Representation for Graphs, with Applications to Molecules. *arXiv e-prints* **2018**, arXiv:1806.09206.

(32) Swann, E.; Sun, B.; Cleland, D.; Barnard, A. Representing molecular and materials data for unsupervised machine learning. *Molecular Simulation* **2018**, *44*, 905–920.

(33) Öztürk, H.; Ozkirimli, E.; Özgür, A. A novel methodology on distributed representations of proteins using their interacting ligands. *Bioinformatics* **2018**, *34*, i295–i303.

(34) Xu, Z.; Wang, S.; Zhu, F.; Huang, J. Seq2seq fingerprint: An unsupervised deep molecular embedding for drug discovery. Proceedings of the 8th ACM International Conference on Bioinformatics, Computational Biology, and Health Informatics. 2017; pp 285–294.

(35) Kuzminykh, D.; Polykovskiy, D.; Kadurin, A.; Zhebrak, A.; Baskov, I.; Nikolenko, S.; Shayakhmetov, R.; Zhavoronkov, A. 3d molecular representations based on the wave transform for convolutional neural networks. *Molecular Pharmaceutics* **2018**, *15*, 4378–4385.

(36) Shi, T.; Yang, Y.; Huang, S.; Chen, L.; Kuang, Z.; Heng, Y.; Mei, H. Molecular image-based convolutional neural network for the prediction of ADMET properties. *Chemosometrics and Intelligent Laboratory Systems* **2019**, *194*, 103853.

(37) Özçelik, R.; Öztürk, H.; Özgür, A.; Ozkirimli, E. ChemBoost: A chemical language based approach for protein-ligand binding affinity prediction. *arXiv e-prints* **2018**, arXiv:1811.00761.

(38) Mikolov, T.; Chen, K.; Corrado, G.; Dean, J. Efficient Estimation of Word Representations in Vector Space. *arXiv e-prints* **2013**, arXiv:1301.3781.

(39) Duvenaud, D. K.; Maclaurin, D.; Iparraguirre, J.; Bombarell, R.; Hirzel, T.; Aspuru-Guzik, A.; Adams, R. P. Convolutional Networks on Graphs for Learning Molecular Fingerprints. Advances in Neural Information Processing Systems. 2015; pp 2224–2232.

(40) Segler, M. H.; Kogej, T.; Tyrchan, C.; Waller, M. P. Generating focused molecule libraries for drug discovery with recurrent neural networks. *ACS Central Science* **2018**, *4*, 120–131.

(41) Popova, M.; Isayev, O.; Tropsha, A. Deep reinforcement learning for de novo drug design. *Science Advances* **2018**, *4*, eaap7885.

(42) Hochreiter, S.; Schmidhuber, J. Long short-term memory. *Neural computation* **1997**, *9*, 1735–1780.

(43) Joshi, C. Transformers are Graph Neural Networks. <https://thegradient.pub/transformers-are-graph-neural-networks/>, 2020.

(44) Wang, S.; Guo, Y.; Wang, Y.; Sun, H.; Huang, J. SMILES-BERT: large scale unsupervised pre-training for molecular property prediction. Proceedings of the 10th ACM International Conference on Bioinformatics, Computational Biology and Health Informatics. 2019; pp 429–436.

(45) Devlin, J.; Chang, M.-W.; Lee, K.; Toutanova, K. BERT: Pre-training of Deep Bidirectional Transformers for Language Understanding. *arXiv e-prints* **2018**, arXiv:1810.04805.

(46) Lipinski, C. A. Lead- and drug-like compounds: the rule-of-five revolution. *Drug Discovery Today: Technologies* **2004**, *1*, 337–341.

(47) Landrum, G. RDKit: open-source cheminformatics <http://www.rdkit.org>. 2016.

(48) Dalke, A. DeepSMILES: An Adaptation of SMILES for Use in Machine-Learning of Chemical Structures. 2018.

(49) Schwaller, P.; Gaudin, T.; Lanyi, D.; Bekas, C.; Laino, T. “Found in Translation”: predicting outcomes of complex organic chemistry reactions using neural sequence-to-sequence models. *Chemical Science* **2018**, *9*, 6091–6098.

(50) Sharma, S. Activation functions in neural networks. 2017.

(51) Domingos, P. Metacost: A general method for making classifiers cost-sensitive. Proceedings of the Fifth ACM SIGKDD International Conference on Knowledge Discovery and Data Mining. 1999; pp 155–164.

(52) Moody, J.; Hanson, S.; Krogh, A.; Hertz, J. A simple weight decay can improve generalization. *Advances in Neural Information Processing Systems* **1995**, *4*, 950–957.

(53) Kingma, D. P.; Ba, J. Adam: A Method for Stochastic Optimization. *arXiv e-prints* **2014**, arXiv:1412.6980.

(54) Moriwaki, H.; Tian, Y.-S.; Kawashita, N.; Takagi, T. Mordred: a molecular descriptor calculator. *Journal of Cheminformatics* **2018**, *10*, 1–14.

(55) Schölkopf, B.; Tsuda, K.; Vert, J.-P. *Kernel methods in computational biology*; MIT press, 2004.

(56) Pedregosa, F. et al. Scikit-learn: Machine Learning in Python. *Journal of Machine Learning Research* **2011**, *12*, 2825–2830.

(57) Chollet, F. Keras. 2015; <https://github.com/fchollet/keras>, online July 2020.

(58) Abadi, M. et al. TensorFlow: Large-Scale Machine Learning on Heterogeneous Systems. 2015; <http://tensorflow.org/>, Software available from tensorflow.org.

(59) Sokolova, M.; Japkowicz, N.; Szpakowicz, S. Beyond accuracy, F-score and ROC: a family of discriminant measures for performance evaluation. Australasian Joint Conference on Artificial Intelligence. 2006; pp 1015–1021.

(60) Chawla, N. V.; Bowyer, K. W.; Hall, L. O.; Kegelmeyer, W. P. SMOTE: synthetic minority over-sampling technique. *Journal of Artificial Intelligence Research* **2002**, *16*, 321–357.

(61) Tukey, J. W., et al. *Exploratory data analysis*; Reading, Mass., 1977; Vol. 2.

(62) Goodarzi, M.; Dejaegher, B.; Vander Heyden, Y. Feature selection methods in QSAR studies. *Journal of AOAC International* **2012**, *95*, 636–51.

(63) Alsenan, S.; Al-Turaiki, I.; Hafez, A. Autoencoder-based Dimensionality Reduction for QSAR Modeling. 2020 3rd International Conference on Computer Applications & Information Security (ICCAIS). 2020; pp 1–4.

(64) Wu, Z.; Ramsundar, B.; Feinberg, E. N.; Gomes, J.; Geniesse, C.; Pappu, A. S.; Leswing, K.; Pande, V. MoleculeNet: a benchmark for molecular machine learning. *Chemical Science* **2018**, *9*, 513–530.

(65) Musgrave, K.; Belongie, S.; Lim, S.-N. A metric learning reality check. European Conference on Computer Vision. 2020; pp 681–699.

(66) Schick, T.; Schütze, H. It's Not Just Size That Matters: Small Language Models Are Also Few-Shot Learners. *arXiv e-prints* **2020**, arXiv:2009.07118.

(67) Huang, B.; Von Lilienfeld, O. A. Communication: Understanding molecular representations in machine learning: The role of uniqueness and target similarity. 2016.

Graphical TOC Entry

